Regulatory γ1 subunits defy symmetry in functional modulation of BK channels

Vivian Gonzalez-Perez[a], Manu Ben Johny[b], Xiao-Ming Xia[a], and Christopher J. Lingle[a,1]

[a]Department of Anesthesiology, Washington University School of Medicine, St. Louis, MO 63110; and [b]Department of Physiology and Cellular Biophysics, Columbia University, New York, NY 10032

Structural symmetry is a hallmark of homomeric ion channels. Nonobligatory regulatory proteins can also critically define the precise functional role of such channels. For instance, the pore-forming subunit of the large conductance voltage and calcium-activated potassium (BK, Slo1, or KCa1.1) channels encoded by a single KCa1.1 gene assembles in a fourfold symmetric fashion. Functional diversity arises from two families of regulatory subunits, β and γ, which help define the range of voltages over which BK channels in a given cell are activated, thereby defining physiological roles. A BK channel can contain zero to four β subunits per channel, with each β subunit incrementally influencing channel gating behavior, consistent with symmetry expectations. In contrast, a γ1 subunit (or single type of γ1 subunit complex) produces a functionally all-or-none effect, but the underlying stoichiometry of γ1 assembly and function remains unknown. Here we utilize two distinct and independent methods, a Forster resonance energy transfer-based optical approach and a functional reporter in single-channel recordings, to reveal that a BK channel can contain up to four γ1 subunits, but a single γ1 subunit suffices to induce the full gating shift. This requires that the asymmetric association of a single regulatory protein can act in a highly concerted fashion to allosterically influence conformational equilibria in an otherwise symmetric K+ channel.

regulatory subunits | BK channels | stoichiometry | K+ channels | FRET

The functional diversity of many ion channels is influenced by regulatory proteins that coassemble with pore-forming α subunits to define channel function. The stoichiometric basis for regulatory subunit assembly in various channels has often been a challenging issue to resolve but is critically important for assessing how a given regulatory subunit may affect channel function. For the large conductance, voltage- and calcium-activated K+ channel (BK, Slo1, or KCa1.1) (1), there are four β subunit genes (*kcnmb*1–4) encoding tissue-specifically expressed subunits (β1–β4) that affect not only the gating range of BK channels (2, 3) but also inactivation behavior (4–8), pharmacology (4, 9), and cell-specific localization and trafficking (10). γ subunits (γ1–γ4) are a second family of subunits (11, 12) that may regulate Slo family channels (13, 14), although at present only γ1 is unambiguously a BK regulatory subunit in native tissues (11, 15). β and γ subunits are unrelated proteins with differing structural topology (Fig. 1*A*), and specific structural information is unavailable. β subunits contain two transmembrane (TM) segments linked by an extracellular loop bridged by multiple disulfide linkages with intracellular C and N termini (16); γ subunits contain a single TM segment, a cytosolic C terminus, and an extracellular N terminus with a large leucine-rich-repeat-containing (LRRC) motif (12, 17) (Fig. 1*A*). For β subunits, potential positions of TM segments in relation to α subunit TM segments have been proposed (18) (Fig. 1*B*).

Although both β and γ1 subunits can shift BK gating at a given Ca²⁺ concentration to more negative potentials (up to −120 mV for γ1 and −50 to −70 mV for specific β subunits) (Fig. 1 *C* and *D*), they do so in independent (19) and mechanistically distinct ways (11, 20). β subunits coassemble with the tetramerically symmetric pore-forming subunits in an up to 1:1 fashion presumably reflecting the

presence of four identical interaction domains presented by the four α subunits, with each β subunit then contributing in an energetically incremental way to influence channel function (21) (Fig. 1 *E* and *F*). In contrast, regulation by the γ1 subunit occurs in a functionally all-or-none fashion (22) (Fig. 1*E*). An all-or-none effect could arise either from a single elementary γ1 functional unit (e.g., monomer, dimer, or tetramer) being present in a BK complex, from the presence of a single γ1 of four total being sufficient to produce the effect, or because the full gating shift only occurs when four γ1 subunits are present (22) (Fig. 1*F*). Any of these possibilities would be an intriguing departure from β subunit regulation of BK channels. During completion of this work, a recent paper observed that up to four γ1 subunits can be present in each BK channel (23) but left open the question of the stoichiometric basis for all-or-none gating shifts.

Here we utilize two independent approaches to assess α:γ1 stoichiometry, a FRET two-hybrid optical approach and an independent approach in which a β2/γ1 chimeric construct is used in single-channel recordings. Together the two approaches yield compatible conclusions, namely, that BK channels can contain up to four γ1 subunits but that only a single γ1 domain is sufficient to produce the all-or-none gating shift. The results require that the asymmetric assembly of a single γ1 subunit can produce a concerted conformational change in the BK channel to favor the enhanced gating characteristic of the all-or-none effect.

Results

FRET Two-Hybrid Measurements Show That BK Channels Can Contain Up to Four γ1 Subunits. Defining stoichiometry of regulatory subunits in symmetric ion channels can be surprisingly recalcitrant to

Significance

Non–pore-forming regulatory subunits (β and γ) define many cell-specific functional properties of Ca²⁺ and voltage-regulated K+ channels (termed BK channels). For β subunits, the tetramerically symmetric core of pore-forming α subunits can be decorated with one to four β subunits, each conferring an energetically incremental effect on channel gating. Here we define the stoichiometric basis of the all-or-none regulatory effect of the γ1 subunit on BK gating. Using a Forster resonance energy transfer-based optical approach and a functional reporter in single-channel recordings, the results show that although BK channels can contain up to four γ1 subunits, asymmetric assembly of a single γ1 subunit in the BK tetramer produces a concerted effect on channel function to mediate the all-or-none effect.

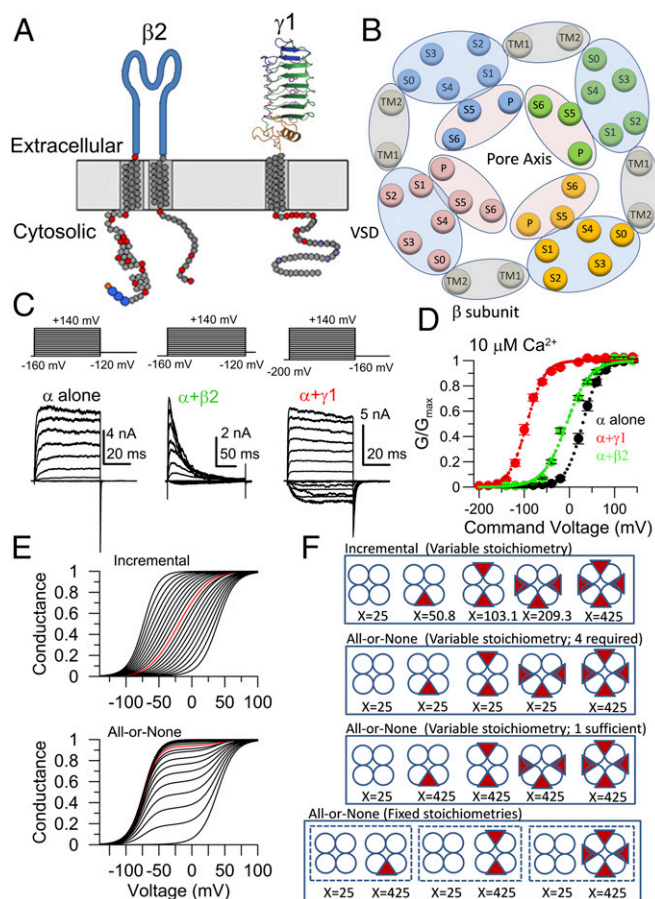**Fig. 1.** Properties of β2 and γ1 subunits of BK channels. (A) Membrane topology of β2 and γ1 regulatory subunits. (B) Schematic of deduced positions of α (S0-P-S6) and β (TM1-TM2) subunit TM segments viewed at the extracellular membrane face (18). Blue ellipse, voltage sensor domain (VSD); pink ellipse, pore domain; gray ellipse, β subunit TMs. (C) Example currents from BK channel expression in oocytes: (*Left*) α alone, (*Center*) α + β2, and (*Right*) α + γ1, with 10 μM intracellular [Ca^{2+}]. Voltage protocols are on top. (D) Conductance–voltage (G–V) curves with Boltzmann fits (dotted lines) for α alone (V_h = 29.4 ± 2.9 mV, z = 1.4 ± 0.1e, mean ± SEM of 10 patches), α + β2 (measured from peak, V_h = −6.3 ± 2.1 mV, z = 1.0 ± 0.03e, mean ± SEM of 10 patches), and α + γ1 (V_h = −94.7 ± 2.7, z = 1.4 ± 0.04e, mean ± SEM of 12 patches) all at 10 μM Ca^{2+}. (E) G–V curves for a BK channel population were simulated with an HA model (36) in which an auxiliary subunit influences allosteric constant, D (22). Curves shift leftward as mole fraction of auxiliary subunits in population increase: (*Top*) each auxiliary subunit in channel complex incrementally influences the allosteric constant [β subunit effect (21)] and (*Bottom*) a single auxiliary subunit (or complex) produces an all-or-none effect on BK gating [γ1 subunit effect (22)]. Red lines correspond to average mole fraction of 0.5, i.e., two auxiliary subunits per four α subunits. (F) Schematized channel assemblies for regulatory subunits acting in an incremental fashion (first panel), an all-or-none fashion with variable stoichiometry with either one subunit sufficient or four required (second and third panels), or an all-or-none fashion with fixed stoichiometric combinations (fourth panel), where X reflects the value of allosteric constant D, used in simulations of E.

straightforward resolution (24–27). We first employ a FRET two-hybrid approach to measure FRET efficiencies between fluorophore-tagged α subunits and the two regulatory subunits. This method leverages an asymmetry in FRET efficiencies measured either as a fractional increase in acceptor fluorescence (E_A, an acceptor-centric measure) or as a fractional quenching of donor emission (E_D, a donor-centric measure). Maximal FRET efficiencies are estimated using both acceptor-centric ($E_{A,max}$) and donor-centric ($E_{D,max}$) measurements at saturating concentrations of free donors (D_{free}) and free acceptors (A_{free}),

respectively. Although both measures are proportional to the expected number of energy transfer events in the bound complex given that all donors are excited, $E_{A,max}$ normalizes this quantity to the number of acceptors (n_A) in the complex, whereas $E_{D,max}$ normalizes it to the number of donors (n_D) in the complex. Thus, the stoichiometry of the bound complex ($\nu = n_D/n_A$) can be estimated as the ratio $E_{A,max}/E_{D,max}$ as has been validated experimentally for ECFP–EYFP concatemers and for myosin Va interaction with calmodulin (28). We tagged the BK Slo1 α subunit with EYFP in either of two positions, the C terminus (tail) or the linker separating the two Ca^{2+}-binding domains. The linker tolerates insertions with minimal functional effect (29, 30). The γ1 subunit cytosolic C terminus was tagged with CFP (as was the β2 C terminus) and mediated normal γ1-like gating shifts when expressed in oocytes (*SI Appendix*, Fig. S1 *A–D*). HEK cells were transfected with γ1-CFP and Slo1-YFP plasmids at different γ1:α ratios and acceptor-centric (E_A) and donor-centric (E_D) FRET was determined. Coexpression of Slo1-EYFP(linker) with γ1-CFP resulted in a maximal acceptor-centric measurement FRET efficiency (E_{Amax}) that was indistinguishable from the maximal donor-centric measure of FRET efficiency ($E_{D,max}$) (Fig. 2 *A* and *B*). Similar results were also obtained for the Slo1-EYFP(tail):γ1-CFP pair (Fig. 2 *D* and *E*), although at reduced absolute FRET efficiencies. The equivalence of $E_{A,max}$ and $E_{D,max}$ estimates for both Slo1 donor constructs (Fig. 2 *B* and *E*) indicates that in both cases, the stoichiometry ratio $\upsilon = E_{A,max}/E_{D,max} \sim 1$ (Fig. 2 *C* and *F*). Thus, there are an equal number of donors and acceptors in the α:γ1 bound complex (i.e., $n_D/n_A \sim 1$). Thus, a BK channel complex can contain up to four γ1 subunits. As expected (21), α and β2 coassembly was also 1:1 (Fig. 2 *C* and *F* and *SI Appendix*, Fig. S2). Although the fact that both donor and acceptor molecules are membrane-associated and FRET signals will likely arise from channel complexes both on surface and intracellular membranes (*SI Appendix, SI Text*), the 1:1 ratio supports two points important for results presented below. First, the CFP-containing regulatory subunit donors do not appear to assemble in a BK complex with more than one regulatory subunit per BK α subunit, and second, the FRET results exclude the possibilities that the all-or-none gating shifts arise from fixed stoichiometries of only one or perhaps two γ1 subunits per channel (Fig. 1F, *Bottom*). The 1:1 γ1:α ratio is consistent with the recent paper, utilizing lanthanide resonance energy transfer, which concluded that up to four γ1 subunits can be present each BK channel (23).

The FRET results indicating that BK channels can contain up to four γ1 subunits per channel still leave open several possibilities for γ1-mediated all-or-none gating shifts. First, all γ1-containing BK channels may contain only a fixed set of four γ1 subunits. Second, channels may accommodate one to four γ1 subunits, but all four are necessary to produce the gating shift. Third, a channel may accommodate zero to four γ1 subunits, but one γ1 is sufficient to produce the all-or-none effect (Fig. 1 *E* and *F*). For the β2 subunit, the problem of stoichiometry was addressed by taking advantage of specific inactivation properties of the β2 subunit (Fig. 1*C*), mediated by its cytosolic N terminus (4, 5, 31). Single α + β2 channels exhibit one of four distinct inactivation rates (21), indicative of the presence of one to four β2 subunits. The inactivation time constant (τ_i) varies in a fashion consistent with each β2 N terminus independently accessing the position of inactivation, with rates of inactivation arising from two, three, or four subunits being twofold, threefold, or fourfold faster than from a single β2 subunit (21). τ_i therefore directly reflects β2:α subunit stoichiometry. In contrast to the −120-mV leftward gating shift produced by the γ1 subunit at all [Ca^{2+}], β2 produces little gating shift at 0 Ca^{2+}. Thus, the presence of a γ1 subunit in a channel can be readily discerned by examination of the likelihood of activation at 0 Ca^{2+}.

A β2/γ1 Chimeric Construct Reveals That the Presence of only a Single γ1 Functional Domain Is Sufficient to Produce the Full All-or-None Gating Shift. Recently, a β1γ1 chimeric construct helped establish that the TM1 segment of γ1 along with a portion of the γ1
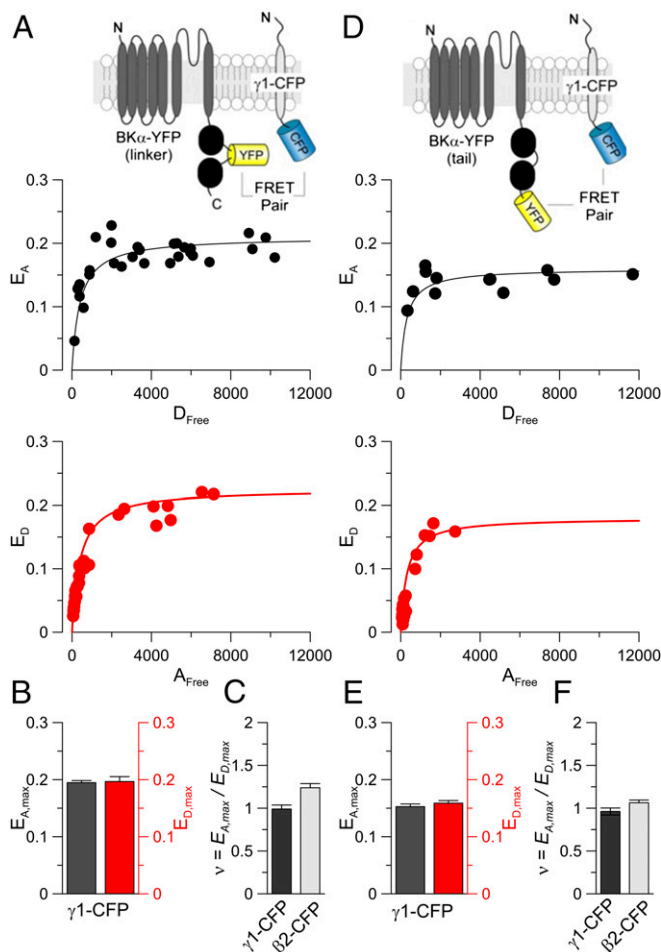
Fig. 2. FRET two-hybrid assay reveals that up to four γ1 subunits are present in a single BK channel. (A) FRET efficiency was determined with the EYFP donor inserted in the linker of the BK α subunit and the ECFP acceptor on the C terminus of the γ1 subunit (Top). (Middle) The 3^3-FRET efficiency (E_A) is plotted against estimated free donor concentration (D_{free}) with each point representing a single cell. (Bottom) E-FRET efficiency (E_D) is plotted as a function of estimated free acceptor concentration (A_{free}). Solid lines are fits of $E_D(D_{free}) = E_{max}[D_{free}/(K_d + D_{free})]$. (B) Mean (±SEM) values for (Left) $E_{A,max}$ and(Right) $E_{D,max}$ for FRET pairs shown in A. (C) The stoichiometry ratio computed as $E_{A,max}/E_{D,max}$ is plotted for FRET pairs between EYFP inserted in the BK linker with either γ1-ECFP or β2-ECFP. $\upsilon \sim 1$ suggests that the ratio of donor to acceptor molecules in the bound complex is 1. (D) Panels show results similar to those in A but for an EYFP donor on the C terminus of the BK α subunit. (E) Mean (±SEM) values for $E_{A,max}$ and $E_{D,max}$ for FRET pairs shown in D. (F) The stoichiometry ratio is plotted for FRET pairs BK α subunit with EYFP attached on the C terminus with γ1-ECFP and β2-ECFP confirming 1:1 stoichiometries.

cytosolic C terminus was sufficient to mediate γ1-induced gating shifts (32). We generated a similar β2γ1 chimera (β2γ1Chim; β2$_{1–194}$:γ1$_{258–298}$; Fig. 3A and *SI Appendix,* Fig. S3A) with the idea that the β2 inactivation domain might provide a functional reporter of stoichiometry of the β2γ1Chim subunit. FRET tests showed that Slo1 α and β2γ1Chim subunits assemble in a 1:1 fashion (*SI Appendix,* Fig. S3 B–F). Currents arising from α plus β2γ1Chim coexpression (Fig. 3B and *SI Appendix,* Fig. S4 G–I) exhibited both β2-like inactivation (*SI Appendix,* Fig. S4 A–C) and γ1-like gating shifts (Fig. 3C and *SI Appendix,* Fig. S4 D–F), whereas the C-terminal tagged β2γ1Chim construct also behaved similarly (*SI Appendix,* Fig. S1 E and F).

Given that the β2γ1Chim construct mediates both β2-like inactivation and γ1-gating shifts, with a limit of four β2γ1Chim subunits per channel, this allowed us to test whether the presence

of a single γ1 domain, embedded in each β2γ1Chim construct, was sufficient to produce the all-or-none gating effect. To accomplish this, we recorded single α + β2γ1Chim channels arising from expression of varying β2γ1Chim:α subunit RNA ratios (Fig. 4 A–D). For 26 single-channel patches, all β2γ1Chim-containing channels exhibited inactivation, and all such channels exhibited a high likelihood of opening during depolarization to +100 mV with 0 Ca^{2+} intracellular solution (Fig. 4 A–D and G and *SI Appendix,* Fig. S5E). The presence of inactivation confirms that a β2 inactivation domain is associated with a given channel. The high likelihood that an opening is observed at +100 mV in 0 Ca^{2+} supports the presence of a γ1-mediated gating shift, as also seen for α + γ1 and α + β2 + γ1 channels but not for α + β2 alone (*SI Appendix,* Fig. S5 B–D).

For each single-channel patch, ensemble averages of the openings activated at +100 mV with 0 Ca^{2+} were generated (Fig. 4 A–D), and τ$_i$ was measured and binned (Fig. 4 E and F). Using previously established criteria (19) (*Materials and Methods*), we examined the ability of three- and four-component Gaussian functions to describe the distributions (*SI Appendix,* Fig. S6). Based on the idea that each inactivation domain in a channel complex acts independently (21), the faster components will bear a simple arithmetic relationship to the slowest component. Furthermore, the SD (σ$_n$) for faster components should be smaller than for slower components, such that σ$_1 \geq$ σ$_2 \geq$ σ$_3 \geq$ σ$_4$, where σ$_1$ corresponds to the slowest component (19). Using these criteria, a four-component Gaussian yielded a better fit (*Materials and Methods*) to the τ$_i$ distribution (Fig. 4 E and F), indicative that one to four β2γ1Chim subunits can be present in a single BK channel, whereas the three-component Gaussian tended to force a larger than expected SD on faster components, and the mean values did not scale with the expected relationship. This independently supports the FRET-based conclusion that up to four γ1 domains can be present in a BK channel. For those channels that inactivated with the slowest τ$_i$ (~55 ms) reflecting the presence of a single β2γ1Chim subunit, the likelihood of opening at +100 mV with 0 Ca^{2+} is comparable to that for channels containing four β2γ1Chim subunits (Fig. 4G). Furthermore, open probability/V curves generated for channels with either one or four β2γ1Chim subunits were
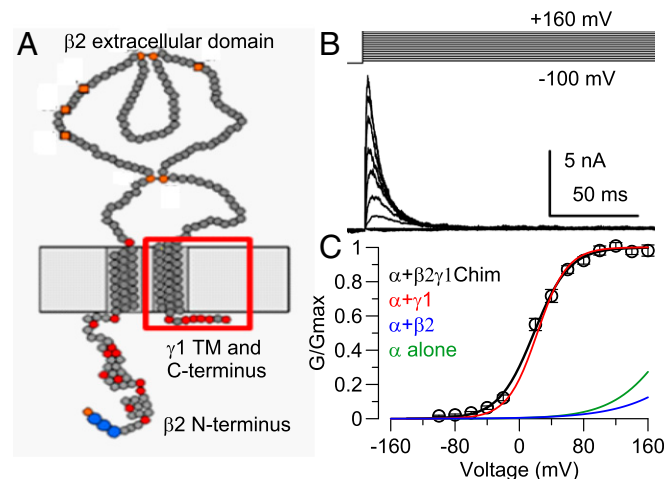

Fig. 3. A β2γ1 chimeric construct produces both β2-like inactivation and γ1-like gating shifts. (A) Cartoon shows the topology of the β2γ1Chim construct containing the inactivating N terminus, TM1, and extracellular segment of β2 with the γ1 TM and cytosolic C terminus (red square) appended. (B) Macroscopic α + β2γ1Chim currents from coexpression of α + β2γ1Chim are shown for activation at 0 Ca^{2+} with indicated protocol. (C) Points plot G–V curve from α + β2γ1Chim peak currents (V$_h$ = 18.4 ± 3.2 mV, z = 1.2 ± 0.1e, n = 10 patches). Solid lines, Boltzmann fits for α + γ1 (V$_h$ = 22.4 ± 2.8 mV, n = 10), α + β2 (241.8 ± 6.3 mV, n = 10), and α alone (V$_h$ = 196.5 ± 5.7 mV, n = 10), all at 0 Ca^{2+}.
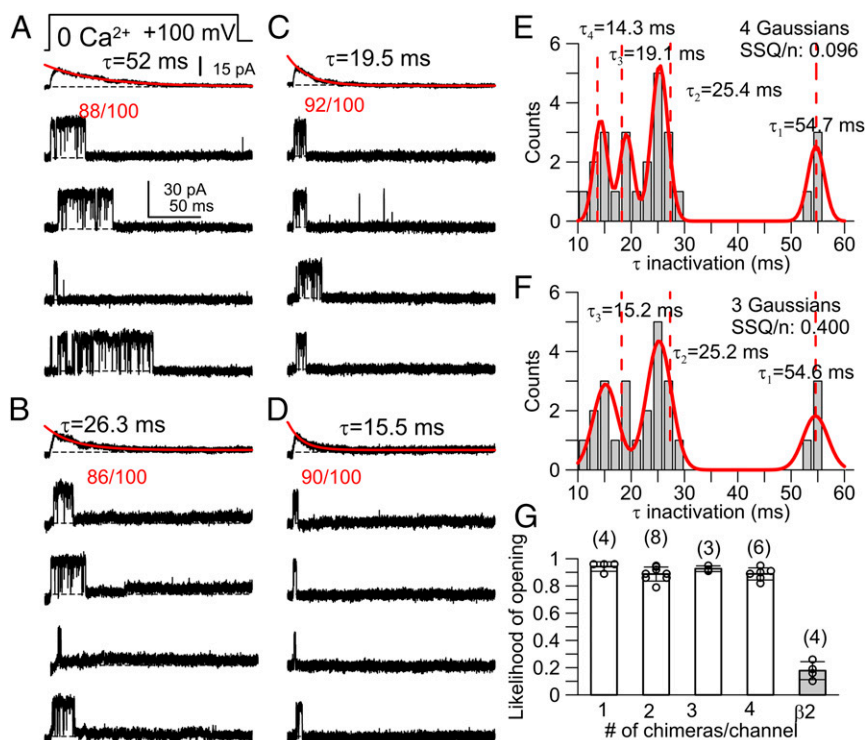
Fig. 4. $\alpha + \beta 2\gamma 1$Chim BK channels show that up to four subunits can be present in a single channel, but one subunit suffices to produce $\gamma 1$-like gating shifts. (*A–D*) Consecutive races from single-channel patches (at 0 Ca^{2+}) from different $\alpha{:}\beta 2\gamma 1$Chim injection ratios, along with ensemble current average from at least 100 total traces. An opening in essentially every sweep at 0 Ca^{2+} indicates a $\gamma 1$ gating shift (numbers show sweeps with openings over total sweeps). (*E* and *F*) Binned distribution of τ_{inact} from 26 single channels (bin size is 2 ms). Red lines represent fits of four-component (*E*) or three-component (*F*) Gaussian distributions, with mean time constants from fits given on the panels and other details given in *SI Appendix, SI Methods*. Vertical dotted lines correspond to predictions for τ_2, τ_3, and τ_4 calculated from 0.5, 0.33, or 0.25 times τ_1. (*G*) For each patch, mean likelihood of observing (*SI Appendix*, Fig. S5) an opening during activation step is shown. Whereas opening likelihood at +100 mV with 0 Ca^{2+} is 0.18 $\pm$ 0.07 for $\alpha + \beta 2$, all $\beta 2\gamma 1$Chim channels have an average likelihood of opening of 0.89 or higher. Number of patches is shown. Likelihood of opening for $\alpha + \beta 2$ differs from all $\beta 2\gamma 1$Chim combinations at $P < 0.01$ (*t* test), with no difference among $\beta 2\gamma 1$Chim groupings. Properties of α alone or $\alpha + \gamma 1$ openings under identical conditions are presented in *SI Appendix*, Fig. S5.

indistinguishable, also indicating that a single $\gamma 1$ domain produces the all-or-none gating shift (*SI Appendix*, Fig. S7).

Competition Between WT $\beta 2$ and Inactivation-Removed $\beta 2\gamma 1$Chim also Indicates That Presence of a Single $\gamma 1$ Domain Is Sufficient to Produce the All-or-None Gating Shift. Although both the $\beta 2$-type inactivation behavior and the $\gamma 1$ shift behavior are retained in the $\beta 2\gamma 1$Chim construct, a concern is that some $\beta 2\gamma 1$Chim subunits might assemble in a fashion that produces independent $\beta 2$ and $\gamma 1$ effects, perhaps compromising conclusions regarding $\gamma 1$ domain stoichiometry. This concern is partly assuaged by the fact that FRET tests (*SI Appendix*, Fig. S3) exclude the possibility that more than four $\beta 2\gamma 1$Chim subunits assemble in a channel. Furthermore, in addition to the 26 single-channel patches obtained with $\beta 2\gamma 1$Chim expression, we observed no single channels which exhibited a gating shift but no inactivation. We did observe one inactivating channel, which initially was readily activated at +100 mV and 0 Ca^{2+} but which later became quiescent under such conditions. This is reminiscent of the rundown of the $\gamma 1$ effect noted in earlier work (22). On balance, it appears that any individual $\beta 2\gamma 1$Chim reliably mediates both $\beta 2$- and $\gamma 1$-like effects. However, it seems possible that a chimeric construct linking domains of different molecular entities together might behave in unexpected ways, undermining the conclusion that only a single $\gamma 1$ domain is sufficient to produce a gating shift.

To address this issue, we undertook a competition test between WT $\beta 2$ subunits and inactivation-removed $\beta 2\gamma 1$Chim subunits [$\beta 2\gamma 1$Chim^{IR} (removal of first 20 N-terminal residues in the $\beta 2$ inactivation domain)]. Knowing that a maximum of four $\beta 2\gamma 1$Chim subunits can be present in a BK channel (*SI Appendix*, Fig. S3), we reasoned that if the $\beta 2\gamma 1$Chim can reliably occupy up to four unique positions on a BK channel, coexpression of WT $\beta 2$ and $\beta 2\gamma 1$Chim^{IR} subunits should result in competition between the two subunits for channel occupancy. This potentially allows a fully independent test of the stoichiometry of the gating shift. If competition between WT $\beta 2$ and $\beta 2\gamma 1$Chim^{IR} occurs, we predict five distinct stoichiometries (Fig. 5*A*): a population of inactivating channels (four $\beta 2$ subunits) with low probability of

activation at +100 mV and 0 Ca^{2+}; a second population (four $\beta 2\gamma 1$Chim^{IR} subunits) that shows high probability of opening at +100 mV (with 0 Ca^{2+}) but no inactivation; and finally, three groups of inactivating channels that exhibit a gating shift that can be distinguished by their rates of inactivation. This is, in fact, observed: there are three populations of inactivating channels that open with high likelihood (Fig. 5 *B–D*), a population of noninactivating channels opening at high likelihood at +100 mV with 0 Ca^{2+} (Fig. 5*E*), and then one population of inactivating channels that rarely open at +100 mV with 0 Ca^{2+} (Fig. 5 *F* and *G*). The distribution of inactivation time constants for the shifted, inactivating channels exhibits three clear components (Fig. 5*H*). That a similar high likelihood of opening is observed for each of the three $\beta 2{:}\beta 2\gamma 1$Chim stoichiometries provides an independent test that when only a single $\gamma 1$ domain is present (three WT $\beta 2$ subunits), it is sufficient to provide a full gating shift (Fig. 5*B*). It will be noted that channels with four $\beta 2\gamma 1$Chim^{IR} subunits exhibit fast block, which is absent when even one WT $\beta 2$ subunit is present. We view this as consistent with results indicating that the truncated $\beta 2$ N terminus has some ability to occupy the BK pore, thereby producing low-affinity block, but that the native $\beta 2$ N terminus, when present, can bind in a preinactivated position (33) that may preclude movement of the truncated N terminus of the chimeric subunits into blocking positions.

Finally, we took advantage of the fact that WT $\beta 2$ subunits can compete away $\beta 2\gamma 1$Chim from the Slo1 channel complex to test whether this would also be observed in FRET measurements. As the mole fraction of WT $\beta 2$ (*SI Appendix*, Fig. S8*C*) expressed with $\beta 2\gamma 1$Chim-CFP (*SI Appendix*, Fig. S8*A*) is increased, one would predict that the average limiting $\beta 2\gamma 1$Chim subunits per channel complex should be reduced; that is, the ratio of $E_{A,max}/E_{D,max}$ should no longer approach unity. Compared with the absence of WT $\beta 2$ (*SI Appendix*, Fig. S8*B*), at a 1:1 ratio of $\beta 2{:}\beta 2\gamma 1$Chim the increase in acceptor emission ($E_{A,max}$) is reduced to about half of the decrease in donor emission (*SI Appendix*, Fig. S8*D*). At 4:1 $\beta 2{:}\beta 2\gamma 1$Chim, any change in donor or acceptor emission is essentially undetectable (*SI Appendix*, Fig. S8*E*). The relative changes in $E_{A,max}$ and $E_{D,max}$ (*SI Appendix*, Fig. S8*F*) along with calculation of the effective $\alpha{:}\beta 2\gamma 1$Chim stoichiometry ($\nu = E_{A,max}/E_{D,max}$) (*SI Appendix*, Fig. S8*G*)
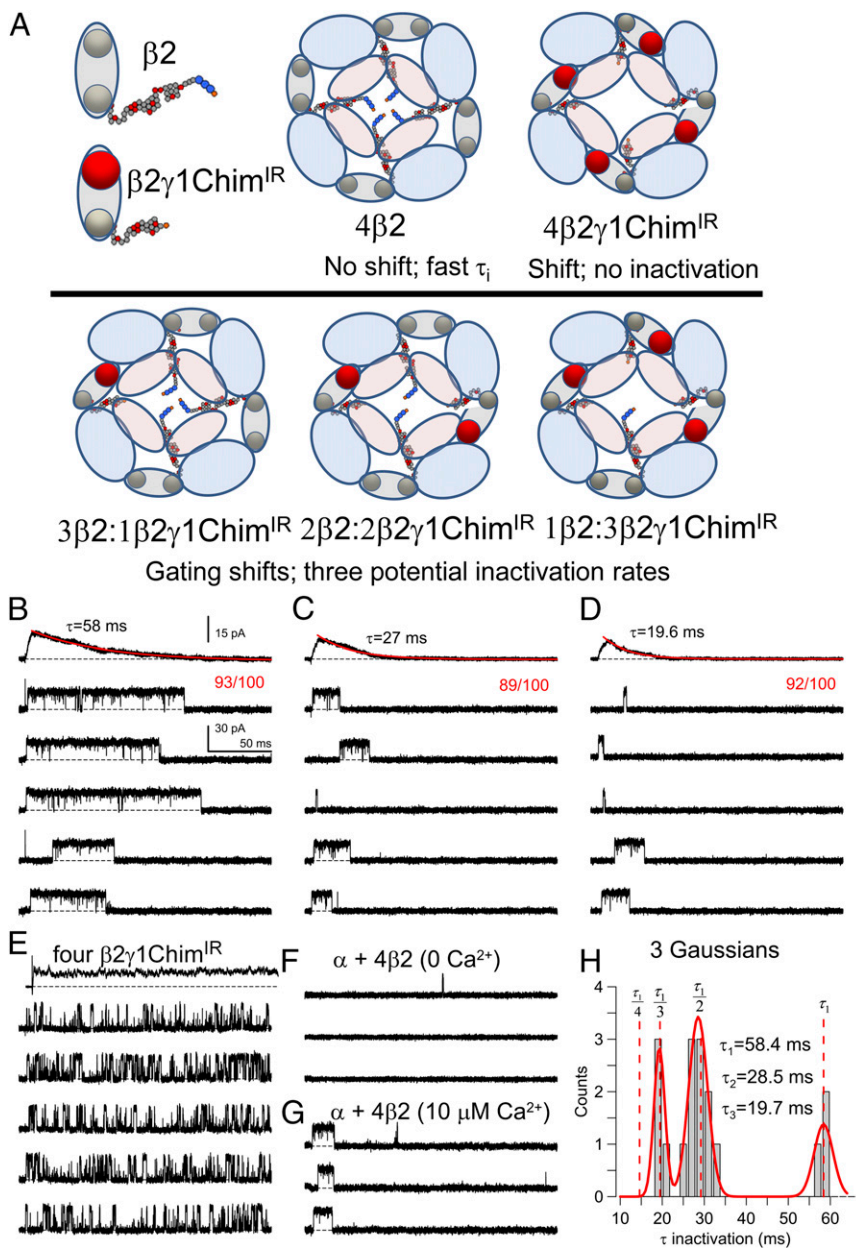
Fig. 5. Competition between WT β2 subunits and inactivation-removed β2γ1Chim[IR] subunits confirms that a single γ1 domain is sufficient to produce γ1-like gating shifts. (A) WT β2 subunit and β2γ1Chim[IR] subunits were coexpressed in different ratios. If WT β2 and β2γ1Chim[IR] subunits compete for channel occupancy, five single-channel stoichiometries are expected. (Top) Channels with four β2 subunits or four β2γ1Chim[IR] subunits. At 0 Ca²⁺, 4β2 channels will rarely open at +100 mV, whereas 4β2γ1Chim[IR] channels will not inactivate but open reliably. (Bottom) Three β2:β2γ1Chim[IR] stoichiometries, 3:1, 2:2, or 1:3, with 3, 2, or 1 available inactivation domains. Inactivating and shifted channels will exhibit one of three inactivation rates. (B) Single channel from group (Fig. 4A) of patches with the slowest τ_i. For B–G, traces were consecutive, and averages of 100 sweeps are at top. Red numbers indicate the number of traces that showed an opening reflecting the likelihood of opening under a given presumed stoichiometry. (C) Single channel with intermediate τ_i. (D) Channel with fast τ_i. (E) A channel with four β2γ1Chim[IR] subunits: no inactivation but high opening likelihood. The truncated N terminus of β2γ1Chim[IR] itself produces fast block, only observed when no WT β2 subunits are present. (F and G) A channel with four β2 subunits rarely opens at +100 mV with 0 Ca²⁺ but robustly activates and inactivates (G) with 10 μM Ca²⁺. In the set of channels from β2 + β2γ1Chim[IR] coexpression, five patches were obtained with β2 inactivation and no gating shift. (H) Distribution of inactivation τ_i (27 patches) is best fit with a three-component Gaussian, whereas a four-component Gaussian failed to fit the data. $\tau_1 = 58.4 \pm 1.8$ ms; $\tau_2 = 28.5 \pm 0.1$ ms, and $\tau_3 = 19.4 \pm 6.6$ ms, with σ_1, σ_2, and σ_3 of 2.19, 2.19, and 0.47 based on criterion that $\sigma_1 \geq \sigma_2 \geq \sigma_3$. Vertical dotted lines correspond to idealized predictions based on $\tau_4 = 0.25\tau_i$, $\tau_3 = 0.33\tau_1$, and $\tau_2 = 0.5\tau_1$.

support the view that a less than 1:1 stoichiometry can be detected, should it occur. This test shows that the FRET signals originating from the β2γ1Chim-CFP donor in association with YFP-tagged Slo1 occupies a position on the Slo1 complex which can be displaced by WT β2, similar to the results in Fig. 5.

Discussion

The results lead us to the conclusion that the TM segment and associated C terminus of a single γ1 subunit in a BK channel are sufficient to produce the all-or-none effect on BK gating. Additional γ1 subunits apparently have no discernible effect. This requires that a single γ1 subunit produces a highly concerted alteration in the BK gating behavior. Our results do not address mechanistically how this occurs. Previously, it has been shown that the γ1 subunit changes the coupling between BK voltage sensors and pore activation (11). In accordance with this idea, association with a single γ1 subunit may produce a structural change that propagates through all four pore-forming subunits making the pore domain more responsive to activation of each of the four voltage sensors.

Overall, the results indicate that the γ1:α subunit assembly is that expected for a tetramerically symmetric channel, 1:1, but that a single γ1 subunit is sufficient to produce the all-or-none shift. These results pose the intriguing question of how a single γ1 subunit produces a concerted effect on the BK channel.

Another question arising from the present results is that if one γ1 subunit is sufficient to produce a gating shift, why can up to four participate in the full BK complex? This question is unanswered, but some earlier results may relate to this issue. It has been previously observed that in excised inside-out patches, the γ1-induced gating shift runs down over many minutes (22). It is unknown whether this represents simply a loss of effect or whether there may be slow dissociation of α and γ1 subunits. In either case, that rundown for intact γ1 subunits occurs raises the possibility that the γ1 subunit effect may undergo dynamic regulation. If so, that one subunit is sufficient, but four can be present, would define the time course of the rundown process or any run-up, should it occur.

Gonzalez-Perez et al.

Materials and Methods

Constructs. Constructs utilized previously included mouse mSlo1 α (GenBank accession no. NP_034740) (34), human LRRC26 (γ1; GenBank accession no. NP_001013675.1) (13), and human β2 (31) (GenBank accession no. NP_852006.1). The primary chimeric construct β2$_{1-194}$:γ1$_{258-298}$ (termed β2γ1Chim) was generated from the human γ1 and β2 subunits. This construct lacked the final 36 residues of the native γ1 subunit, as utilized previously for a β1γ1Chim construct (32). To make an inactivation-removed (IR) version of β2γ1Chim, termed β2γ1Chim^{IR}, we removed the first 20 residues of the β2 inactivation domain of β2γ1Chim. Two tagged Slo1 constructs were generated. Slo1-YFP(tail) had enhancedYFP (EYFP) appended to the Slo1 C terminus with a short dipeptide (AlaSer) linker. For Slo1-YFP(linker), EYFP was inserted between residues 652 and 653 (...KKKQRN^{652}-TSGG-EYFP-GGVN-G^{653}GMRN....). For γ1-CFP, ECFP was appended to the human γ1 C terminus with an intervening linker: γ1–15G-TG-ECFP. For β2-CFP, ECFP was appended to C terminus of human β2 also with a short intervening linker: β2–5G-ECFP. The β2γ1Chim-ECFP construct was tagged similarly at the C terminus. Coexpression of γ1-ECFP or β2-ECFP with Slo1-EYFP resulted in currents which exhibited the expected γ1 or β2 functional effects (*SI Appendix*, Fig. S1), confirming that the presence of ECFP did not alter the ability of these constructs either to coassemble with Slo1 α subunits or to functional normally.

Expression in Oocytes and Cells. Stage IV *Xenopus laevis* oocytes were used for channel expression for electrophysiological recordings. The cRNAs of all constructs were prepared at ~1 μg/μL. For macroscopic recordings, cRNA mixes containing (molar ratio) mSlo1 alone, mSlo1+ hβ2 (1:6.5), mSlo1+ hLRRC26 (1:4), or mSlo1+β2$_{1-194}$:γ1$_{258-298}$ (β2γ1Chim; 1:6) were diluted 1:5 before injection. For single-channel recordings, mSlo1:β2γ1Chim (1:4) was diluted 1:20–1:100 before injection. Oocytes were used 2–5 d after injection, except for single-channel recordings in which they were used 1–2 d after

injection. HEK293 cells (ATCC) CRL-1573 were grown in DMEM, 10% FCS, and 1% penicillin/streptomycin at 37 °C, 5% CO$_2$. Cells were transfected with polyethylenimine (PEI) 25 kDa linear polymer (Polysciences #2396602) at a 2:1 ratio of PEI (μg) to total DNA (μg) (Invitrogen/Life Technologies). One to two μg of tagged BK α was transfected with 1–2 μg regulatory subunit constructs for expression.

Electrophysiology. Details of pipette preparation and recording methods for similar experiments have been described recently (19). All currents were recorded in the inside-out patch configuration with an Axopatch 200B amplifier (Molecular Devices). Data were acquired with the Clampex program from the pClamp software package (Molecular Devices). The standard frog Ringer using during seal formation included, in mM, 115 NaCl, 2.5 KCl, 1.8 CaCl$_2$, 10 Hepes, at pH 7.4, and after patch excision, the pipette tip was moved into flowing test solutions. The pipette/extracellular solution was, in mM, 140 K-methanesulfonate, 20 KOH, 10 Hepes, 2 MgCl$_2$, at pH 7.0. Solutions for bathing the cytosolic side of the membrane were prepared as described (35), with 140 mM methanesulfonate, 20 mM KOH, 10 mM Hepes, pH adjusted to 7.0. HEDTA was used for 10 μM Ca^{2+} and 5 mM EGTA for 0 μM Ca^{2+}solutions. The 10 μM Ca^{2+} solution was adjusted to appropriate pCa with Ca-Mes, and solutions of defined Ca^{2+} concentrations (World Precision Instruments) were used to calibrate the 10-μM solution using a Ca^{2+}-sensitive electrode. A large bore perfusion pipette tip containing multiple independent solution lines was used to apply test solutions directly to patches. Experiments were at room temperature (~22–25 °C). Salts and buffers were obtained from Sigma. Additional details of measurement and analysis of gating shifts and fitting of distributions are in *SI Appendix*.

1. Butler A, Tsunoda S, McCobb DP, Wei A, Salkoff L (1993) mSlo, a complex mouse gene encoding "maxi" calcium-activated potassium channels. *Science* 261:221–224.
2. McManus OB, et al. (1995) Functional role of the beta subunit of high conductance calcium-activated potassium channels. *Neuron* 14:645–650.
3. Cox DH, Aldrich RW (2000) Role of the β1 subunit in large-conductance Ca$^{(2+)}$-activated K$^{(+)}$ channel gating energetics. Mechanisms of enhanced Ca$^{(2+)}$ sensitivity. *J Gen Physiol* 116:411–432.
4. Xia X-M, Ding JP, Lingle CJ (1999) Molecular basis for the inactivation of Ca^{2+}- and voltage-dependent BK channels in adrenal chromaffin cells and rat insulinoma tumor cells. *J Neurosci* 19:5255–5264.
5. Wallner M, Meera P, Toro L (1999) Molecular basis of fast inactivation in voltage and Ca^{2+}-activated K$^+$ channels: A transmembrane beta-subunit homolog. *Proc Natl Acad Sci USA* 96:4137–4142.
6. Xia X-M, Ding J-P, Zeng X-H, Duan K-L, Lingle CJ (2000) Rectification and rapid activation at low Ca^{2+} of Ca^{2+}-activated, voltage-dependent BK currents: Consequences of rapid inactivation by a novel β subunit. *J Neurosci* 20:4890–4903.
7. Uebele VN, et al. (2000) Cloning and functional expression of two families of beta-subunits of the large conductance calcium-activated K$^+$ channel. *J Biol Chem* 275: 23211–23218.
8. Zeng X-H, Benzinger GR, Xia XM, Lingle CJ (2007) BK channels with β3a subunits generate use-dependent slow afterhyperpolarizing currents by an inactivation-coupled mechanism. *J Neurosci* 27:4707–4715.
9. Meera P, Wallner M, Toro L (2000) A neuronal beta subunit (KCNMB4) makes the large conductance, voltage- and Ca^{2+}-activated K$^+$ channel resistant to charybdotoxin and iberiotoxin. *Proc Natl Acad Sci USA* 97:5562–5567.
10. Toro B, et al. (2006) KCNMB1 regulates surface expression of a voltage and Ca2+-activated K+ channel via endocytic trafficking signals. *Neuroscience* 142:661–669.
11. Yan J, Aldrich RW (2010) LRRC26 auxiliary protein allows BK channel activation at resting voltage without calcium. *Nature* 466:513–516.
12. Yan J, Aldrich RW (2012) BK potassium channel modulation by leucine-rich-containing proteins. *Proc Natl Acad Sci USA* 109:7917–7922.
13. Yang C, Zeng XH, Zhou Y, Xia XM, Lingle CJ (2011) LRRC52 (leucine-rich-repeat-containing protein 52), a testis-specific auxiliary subunit of the alkalization-activated Slo3 channel. *Proc Natl Acad Sci USA* 108:19419–19424.
14. Zeng XH, Yang C, Xia XM, Liu M, Lingle CJ (2015) SLO3 auxiliary subunit LRRC52 controls gating of sperm KSPER currents and is critical for normal fertility. *Proc Natl Acad Sci USA* 112:2599–2604.
15. Yang C, et al. (2017) Knockout of the LRRC26 subunit reveals a primary role of LRRC26-containing BK channels in secretory epithelial cells. *Proc Natl Acad Sci USA* 114:E3739–E3747.
16. Knaus HG, et al. (1994) Primary sequence and immunological characterization of beta-subunit of high conductance Ca$^{(2+)}$-activated K$^+$ channel from smooth muscle. *J Biol Chem* 269:17274–17278.
17. Dolan J, et al. (2007) The extracellular leucine-rich repeat superfamily; a comparative survey and analysis of evolutionary relationships and expression patterns. *BMC Genomics* 8:320–343.
18. Liu G, et al. (2010) Location of modulatory beta subunits in BK potassium channels. *J Gen Physiol* 135:449–459.
19. Gonzalez-Perez V, Xia XM, Lingle CJ (2015) Two classes of regulatory subunits coassemble in the same BK channel and independently regulate gating. *Nat Commun* 6: 8341.
20. Hoshi T, Pantazis A, Olcese R (2013) Transduction of voltage and Ca^{2+} signals by Slo1 BK channels. *Physiology* 28:172–189.
21. Wang Y-W, Ding JP, Xia X-M, Lingle CJ (2002) Consequences of the stoichiometry of Slo1 α and auxiliary β subunits on functional properties of large-conductance Ca2+-activated K+ channels. *J Neurosci* 22:1550–1561.
22. Gonzalez-Perez V, Xia XM, Lingle CJ (2014) Functional regulation of BK potassium channels by γ1 auxiliary subunits. *Proc Natl Acad Sci USA* 111:4868–4873.
23. Carrasquel-Ursulaez W, Alvarez O, Bezanilla F, Latorre R (2018) Determination of the stoichiometry between alpha- and gamma1 subunits of the BK channel using LRET. *Biophys J* 114:2493–2497.
24. Nakajo K, Ulbrich MH, Kubo Y, Isacoff EY (2010) Stoichiometry of the KCNQ1–KCNE1 ion channel complex. *Proc Natl Acad Sci USA* 107:18862–18867.
25. Plant LD, Xiong D, Dai H, Goldstein SA (2014) Individual IKs channels at the surface of mammalian cells contain two KCNE1 accessory subunits. *Proc Natl Acad Sci USA* 111: E1438–E1446.
26. Kobertz WR (2014) Stoichiometry of the cardiac IKs complex. *Proc Natl Acad Sci USA* 111:5065–5066.
27. Morin TJ, Kobertz WR (2008) Counting membrane-embedded KCNE beta-subunits in functioning K+ channel complexes. *Proc Natl Acad Sci USA* 105:1478–1482.
28. Ben Johny M, Yue DN, Yue DT (2016) Detecting stoichiometry of macromolecular complexes in live cells using FRET. *Nat Commun* 7:13709.
29. Giraldez T, Hughes TE, Sigworth FJ (2005) Generation of functional fluorescent BK channels by random insertion of GFP variants. *J Gen Physiol* 126:429–438.
30. Miranda P, et al. (2013) State-dependent FRET reports calcium- and voltage-dependent gating-ring motions in BK channels. *Proc Natl Acad Sci USA* 110: 5217–5222.
31. Xia XM, Ding JP, Lingle CJ (2003) Inactivation of BK channels by the NH$_2$ terminus of the β2 auxiliary subunit: An essential role of a terminal peptide segment of three hydrophobic residues. *J Gen Physiol* 121:125–148.
32. Li Q, Guan X, Yen K, Zhang J, Yan J (2016) The single transmembrane segment determines the modulatory function of the BK channel auxiliary γ subunit. *J Gen Physiol* 147:337–351.
33. Benzinger GR, Xia XM, Lingle CJ (2006) Direct observation of a preinactivated, open state in BK channels with β2 subunits. *J Gen Physiol* 127:119–131.
34. Xia X-M, Zeng X, Lingle CJ (2002) Multiple regulatory sites in large-conductance calcium-activated potassium channels. *Nature* 418:880–884.
35. Zhang X, Zeng X, Lingle CJ (2006) Slo3 K$^+$ channels: Voltage and pH dependence of macroscopic currents. *J Gen Physiol* 128:317–336.
36. Horrigan FT, Aldrich RW (2002) Coupling between voltage sensor activation, Ca^{2+} binding and channel opening in large conductance (BK) potassium channels. *J Gen Physiol* 120:267–305.